Medium-Sized Helicopter Noise Abatement Flight Test

Kyle A. Pascioni
NASA Langley Research Center
Hampton, VA, USA

Eric Greenwood*
The Pennsylvania State University
University Park, PA, USA

Michael E. Watts*
Analytical Mechanics Associates, Inc.
Hampton, VA, USA

Charles D. Smith
Analytical Mechanics Associates, Inc.
Hampton, VA, USA

James H. Stephenson
U.S. Army Combat Capabilities Development Command
Aviation & Missile Center
Hampton, VA, USA

ABSTRACT

An extensive flight test campaign was recently completed, which aims to reduce the operational noise generated by helicopters in an effort to improve community acceptance. Using a ground-based microphone array, acoustic measurements were acquired on helicopters in the medium-sized vehicle weight class over a number of flight conditions including steady level flight, steady descents, and approaches. While data were collected across four helicopters, the Leonardo AW139 and Sikorsky S-76D will be the focus of this paper. Source noise hemispheres are computed for the steady test points, but the ground noise contours measured during approach conditions cover only a small portion of the area impacted by noise because of practical constraints on the size of the deployed array. Thus, the Noise Informed Community Environment Operations Planning System (NICEOPS) in conjunction with the flight test data was used to estimate how changes in the approach procedures impact noise exposure over a larger ground area. It was found that even small longitudinal accelerations can have a substantial influence on the noise generation processes during approach and must be modeled appropriately to develop new flight procedures which minimize the acoustic impact on the ground.

INTRODUCTION

The public acceptance of helicopter noise has consistently limited operations within urban areas and surrounding communities (Refs. 1, 2). Broadly speaking, two strategies can be taken to reduce perceived noise at the ground: acoustics-based vehicle design or operational planning. While there is certainly merit in the first option, the tradeoffs with performance, safety, and cost often preclude substantial aeroacoustic improvements. Moreover, implementing a noise reduction technology is typically a lengthy process taking many years before the technology is available on a significant portion of the civil helicopter fleet. This research effort has chosen the second approach with the goal of understanding the noise benefit by tailoring operations of existing vehicles such that ground noise exposure is reduced. This work is part of the NASA Revolutionary Vertical Lift Technology project under the Advanced Air Vehicles Program.

It is common knowledge that helicopter source noise is sensitive to the operating state. Blade-Vortex Interaction (BVI) is often a dominant noise source mechanism and is caused by tip vortices being convected through the main rotor system, introducing impulsive unsteady pressure fluctuations on downstream blades. In turn, those fluctuations can radiate quite efficiently as noise in the far field. Assuming constant drag, weight, and disk loading, peak BVI occurs for specific airspeed-descent rate combinations (Ref. 3). Thus, avoiding BVI through trajectory and path planning has the potential to significantly reduce the resulting ground noise. For example, previous studies have shown a reduction in overall noise, both during approach (Refs. 4, 5) and en route (Refs. 3, 6–8). In addition to BVI, other source mechanisms such as the tail rotor can also contribute to the overall vehicle noise – the extent to which being configuration dependent. Aside from the source itself, geometric considerations of the trajectory can reduce noise exposure during approach to land, e.g., steep angles to get assistance from spherical spreading and moderate speeds to limit duration effects. The balance between these source noise and trajectory implications is an important aspect of operational planning.

Recently, a flight test was conducted involving six lightweight helicopters with Takeoff Gross Weight (TOGW) between 2000-4500 lbs to acquire source noise and compare the noise level over various approach procedures and maneuvers (Ref. 9). As a follow-on, and the focus of this paper, NASA, the FAA, and the US Army recently completed the second phase of these tests to investigate similar noise abatement procedures with medium-sized helicopters. These helicopters include a Sikorsky S-76D, a Leonardo AW139, the US Coast Guard MH-65 Dolphin (a variant of the commercial Airbus AS365 Dauphin), and a Bell 205 “Huey”, in which TOGW

*Formerly NASA Langley Research Center, Hampton, VA

Presented at the *VFS International 76th Annual Forum & Technology Display*, Virginia Beach, Virginia, October 6–8, 2020.

ranged from 7,400-14,200 lbs. Given the constraints of the test site, the extent of the ground-based measurements in the flight direction was limited. Thus, in addition to analysis and discussion of the results, an attempt is made to predict the approach noise contours over a wider area than could be measured using a method currently under development, the Noise Informed Community Environment Operations Planning System (NICEOPS), developed from steady flight noise data collected during the flight test.

The experimental setup will first be discussed, including details of the instrumentation and prescribed flight procedures. Then, the processing methodology for obtaining source hemispheres and measured ground noise contours is presented. Details of the NICEOPS methodology and the experimental database interpolation is also outlined. Finally, results summarizing the measured data and a discussion on the results from the simulated approaches will be given, focusing on the relation to the effective flight path angle during non-constant flight conditions.

TEST DETAILS

Vehicles

Acoustic data were acquired on four medium-sized helicopters. Take-off Gross Weight (TOGW) varied between 7,400 and 14,200 lbs with a main rotor blade count between 2 and 5 driven by turboshaft engines. Three vehicles are equipped with conventional tail rotors, while the MH-65 has a Fenestron.™ Additional characteristics are provided in Table 1. Note that for brevity, results from the AW139 and S-76D will be the focus of this paper. Additional data including the Bell 205 and MH-65 can be found in Refs. 10, 11.

Instrumentation

An array of 39 microphones (1/2-inch GRAS 67AX) flush-mounted to ground boards were distributed across the field spanning approximately 4,000 ft by 2,000 ft perpendicular and parallel to the flight path, respectively, as shown in Figure 1. Their locations were chosen to provide good coverage for source noise characterization, maneuvering flight, and to obtain ground noise footprints during noise abatement approaches. The airfield was reasonably flat with a maximum ellipsoid elevation difference of 38 ft between any two microphones. Acquisition of the acoustic signals employed the second generation NASA Wireless Acoustic Measurement System (WAMS2), which digitized each signal at 25 kS/s via a single channel 24-bit analog to digital delta-sigma converter with built-in antialiasing. The data were streamed with Universal Coordinated Time (UTC) GPS stamps to an SD memory card. Each WAMS2 unit supported a single microphone station and provided wireless control, system health monitoring, and upon request, a synopsis of the acoustic data collected during the last run.

Wind speed and direction, pressure, temperature, and humidity were recorded every six seconds at five ground stations distributed across the field. Wind speed and direction were also measured as a function of elevation at a single ground position near the flight path via a ZephIR 300 portable LIDAR system (see Figure 1). The primary use of the gathered weather information was to monitor environmental conditions to ensure they were within reason to obtain quality data. These data were also used as inputs for an atmospheric attenuation model when building the source hemispheres (see Processing Methods section). Wind was the primary concern and was desired to be less than 10 kts sustained at elevation. If large vertical gradients were observed from the LIDAR measurement, test points that called for minimal altitude variations were flown to minimize airspeed uncertainty.

A four lamp Precision Approach Path Indicator (PAPI) system provided the pilot with a visual reference to maintain the prescribed slope during constant flight path angle descents. This system is an extended version of the previous two lamp system (Ref. 9) and controlled using the same principles. Each lamp angle was remotely adjusted according to the desired flight path angle and displayed viewing-angle-dependent white/red patterns to notify the pilot if they were too low, too high, or on slope.

On board the test vehicles, the Aircraft Navigation and Tracking System (ANTS2), the successor of ANTS (Ref. 9), gathered vehicle position and state information. ANTS2 is equipped with a VectorNav VN-310 dual antenna GPS Inertial Navigation System (INS) with an internal Extended Kalman Filter to calculate the aircraft state solution. UTC stamps were also recorded to relate and synchronize the vehicle position and state to the acoustic data during postprocessing. The GPS position was adjusted so the coordinate system origin coincides with the array center microphone, station 16 in Figure 1. Nominal horizontal and vertical root-mean-square uncertainty in position are 5 ft and 16 ft, respectively.

Flight Procedures

Steady flights were performed for source characterization, i.e., to form acoustic hemispheres. Level flights ranged from 40 to V_H (maximum speed at maximum continuous power) knots indicated airspeed (KIAS) at a target altitude of 200 ft Above Ground Level (AGL). Steady descents from 60 to 100 KIAS at -3 to -12 degrees were also tested. The initial altitude was set such that the termination of the run was at the end of the array near the PAPI system. Climbs at the best rate of climb, V_y, and $V_y \pm 10$ KIAS, were also included. A number of noise abatement approach procedures were formed by defining an entry speed, flight path angle, and altitude, followed by an AGL point to initiate various descent rates while maintaining the initial flight path angle.

Several maneuvers involving bank angles between 20° and 45° into and away from the advancing side were also performed. Prior to the initiation of the turn, a number of initial conditions were prescribed (e.g., descents, decelerations, etc.) to study the effect of wake location on radiated noise. These maneuver data will not be discussed herein, but the reader is referred to Refs. 10, 11.

Table 1. Aircraft Characteristics.

Manufacturer	Bell	Leonardo	Sikorsky	Eurocopter
Model	205 “Huey”	AW139	S-76D	MH-65
TOGW (lbs)	7460	14,200	11,370	9,530
No. of Turboshaft Engines	1	2	2	2
MR Blades	2	5	4	4
MR Diameter (ft)	48.27	45.25	44	39.08
MR Blade Passage Frequency (Hz)	11	24	21	24
TR Type	2-bladed	4-bladed	4-bladed	Fenestron™

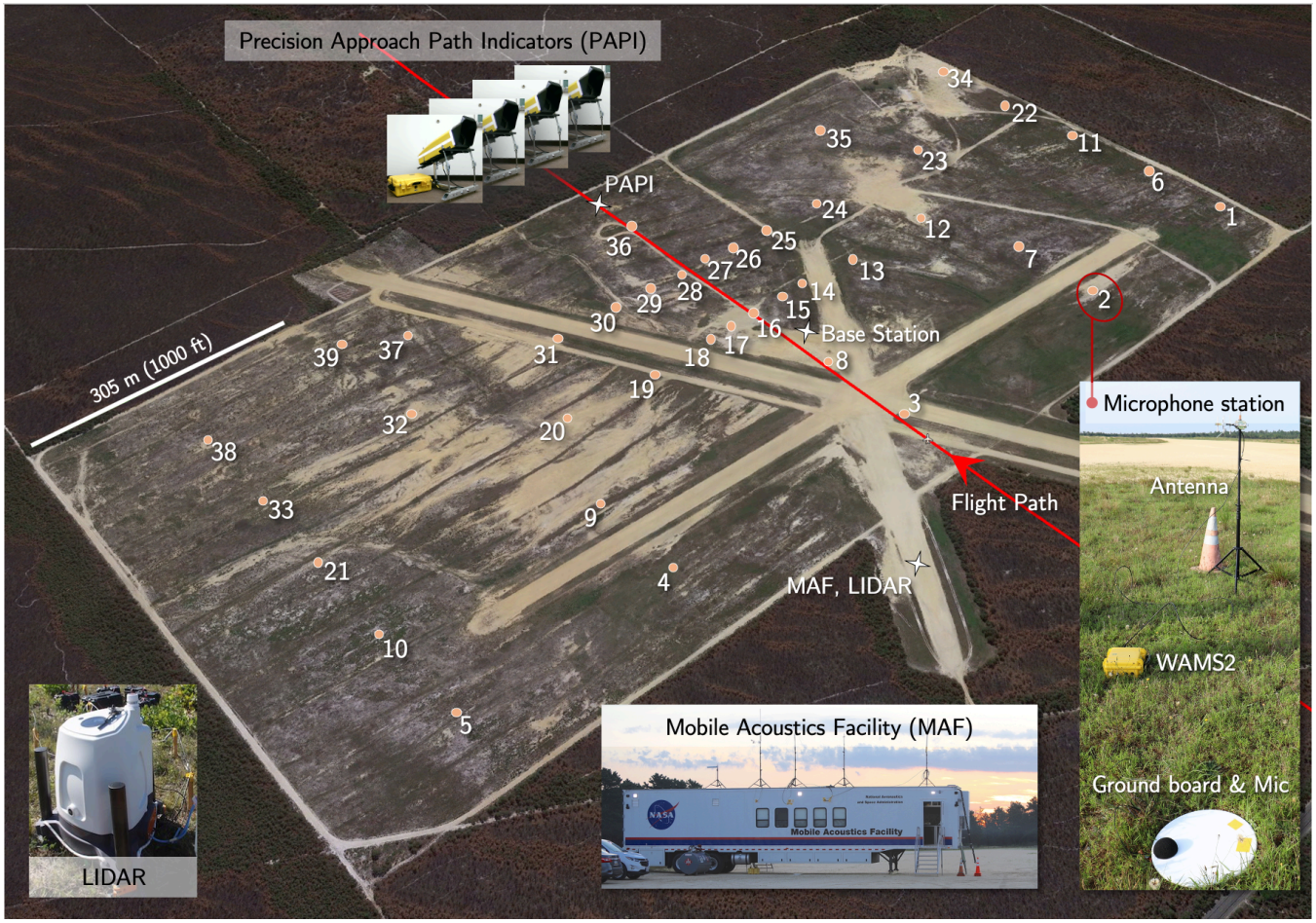

Figure 1. Bird’s eye view of Coyle Field, NJ, displaying microphone locations and supporting test equipment. The nominal flight path is shown in red.

PROCESSING METHODS

Source Hemispheres

Acoustic hemispheres are created for each level flight, climb, and steady descent test point using the Acoustic Repropagation Tool (ART) methodology contained within the Advanced Acoustic Model (AAM), formerly the Rotorcraft Noise Model (Refs. 12, 13). While previous flight tests (Refs. 9, 14) from NASA have used the same general methodology, some internal modifications have been made that are not documented. Therefore, an overview of the process will now be given.

The pressure time series at each ground microphone are first split into 0.5 second nonoverlapping data segments. For each segment, three Fourier transforms are computed on 0.25 second blocks at 50% overlap. The three transforms are ensemble averaged using a Hamming window, producing a 4 Hz bin-width narrowband spectrum estimate. This process results in independent spectra at every 0.5 second. Prior to back propagation to the hemisphere surface, a number of steps are performed. To start, the spectral amplitude at each frequency for each narrowband spectrum estimate, per microphone, is compared to the lowest level at that same frequency over its spectral-time history for a given run. The lowest levels represent the ambient levels for that run. If the difference in those amplitudes are under some prescribed threshold, the data are removed due to poor signal-to-noise ratio; this reduces falsely back propagating ambient noise. For this work, the threshold is set to 5 dB. It is typical that higher frequencies cannot always meet this criteria due to the lack of radiated noise in this frequency range. In particular, high frequencies at emission angles close to the rotor plane may be attenuated beyond ambient levels by the atmosphere upon traveling long distances.

For this work, the narrowband spectra are converted to one-third-octave bands. AAM is used to compute and remove the effect of spherical spreading, atmospheric attenuation, and ground losses. For atmospheric attenuation, the medium is assumed to be isotropic, and the ANSI S1.26 (Ref. 15) model is applied based on the center band frequencies given temperature, pressure, and humidity from an average of the WAMS2 weather station data. Characteristic impedance of the ground is estimated through the single parameter Delany & Bazley model (Ref. 16) assuming a ground flow resistivity of 200 CGS Rayls, a value typical of soft ground. Given this information, the model by Chien and Soroka (Ref. 17) is used to estimate the angle and frequency dependent ground losses. It should be noted that the pressure doubling effects of the microphone installation and the ground board are not removed.

With knowledge of the aircraft position from the tracking data, each one-third-octave band spectra at each microphone, now free of propagation effects can be back propagated to form a 100 ft radius discretized source hemisphere centered at the onboard GPS receiver using straight rays between the observer and vehicle location at the time of emission. Uniform grid spacing between sound pressure data points on the hemisphere is desired for convenience when using the hemispheres. Thus, data are interpolated onto a structured grid with 10° and 5° spacing the elevation and azimuth directions, respectively, using Shepard's inverse distance weighting (Ref. 18) with a radius of influence corresponding to 30° range in both directions. Overall metrics (e.g., dBA, BVISPL, etc.) can then be computed on the structured grid by integrating the frequency spectra. The hemisphere data are given herein in the form of Lambert projections for minimal contour distortion.

Measured Ground Noise Contours

The steady source assumption no longer holds for the noise abatement approaches since the aerodynamic state (hence, the acoustic state) changes while the vehicle decelerates. Thus, ground noise contours are used to represent the measured data. The A-weighted sound exposure level (SEL) is computed at each microphone and is spatially interpolated to form the contours. Note that this metric is computed using the measured data. That is, corrections (e.g., atmospheric attenuation, ground losses, etc.) which were applied to the source hemispheres are not used here.

Simulated Ground Noise Contours

The measured ground noise contours cover only a small portion of the area impacted by noise during the approach procedures because of practical constraints on the size of the deployed acoustic array. An aircraft noise prediction method currently under development at Penn State called the Noise Informed Community Environment Operations Planning System (NICEOPS) was used to estimate how changes in operating procedures impact noise exposure over a wider area. NICEOPS is intended for applications where rapid predictions of aircraft acoustic impacts are required, for instance the real time display of aircraft noise emissions to operators and airspace managers or for the design and near-real-time optimization of noise abatement flight procedures. To accelerate the computation of acoustic impacts, NICEOPS uses a precomputed database of aircraft noise radiation characteristics that describe how the frequency and magnitude of the noise radiated to the far-field vary with the aerodynamic operating condition of the vehicle. For conventional helicopters, these source noise data are applied quasistatically for each point in time based on the estimated aerodynamic operating condition of the main rotor. The main rotor operating condition is determined from the vehicle's inertial velocity and acceleration along the trajectory using a method substantially similar to that described in Ref. 19. The rotor operating condition is defined by the hover tip Mach number, M_H, advance ratio, μ, thrust coefficient, C_T, and steady-flight effective flight path angle, γ_e. The thrust coefficient during maneuvering flight is determined by scaling the weight coefficient by the load factor due to acceleration, e.g.,:

$$C_T = C_W \, |\vec{n}| \tag{1}$$

where the net acceleration vector is defined as:

$$\vec{n} = a_x \hat{i} + a_y \hat{j} + (a_z + 1)\hat{k} \tag{2}$$

where a_i are the inertial accelerations in g's and z is aligned with gravity. As described in Ref. 19, the orientation of the main rotor tip path plane–and the resulting noise–is assumed to change along with the change in the net acceleration vector.

The effective flight path angle, γ_e, is then defined by the inner product of the unit normal of the net acceleration vector and the velocity vector:

$$\sin\gamma_e = \hat{v}\cdot\hat{n}. \tag{3}$$

When the net acceleration vector is aligned with gravity (e.g., in steady flight), the effective flight path angle is exactly the nominal flight path angle, γ. When the vehicle is accelerating, such that the net acceleration vector has a component aligned with the velocity vector, the effective flight path angle becomes more positive. Likewise, during a deceleration, the effective flight path angle becomes more negative. For moderate accelerations that do not violate the small angle assumption of the original Quasi-Static Acoustic Mapping (Q-SAM) method (Ref. 20), every 0.1 g (less than 2 kts/s) of longitudinal deceleration has the same effect as descending at constant speed along a flight path angle 6° more steeply than the nominal flight path angle.

In this paper, the source noise database was generated from the previously described set of AAM acoustic spheres. Because the range of main rotor operating conditions that are achieved during accelerating flight can easily exceed the range of equivalent steady flight conditions, several heuristics were applied to artificially extend the data, following an approach to extending the noise data set similar to that described in Ref. 21. First, the nondimensional operating conditions $(\mu, C_T, \gamma_e, M_H)$ associated with each of the measured acoustic hemispheres are computed based on the rotor geometry, vehicle gross weight, and ambient temperature and density at the time of data acquisition.

In order to enclose the region of the operating envelope where high BVI noise occurs, level flight conditions where no BVI occurs are replicated in the database at the same advance ratio, but at effective flight path angles of -24° and 35°, covering the range of effective flight path angles that may be achieved during accelerating flight. The effects of rotor thrust variation are approximated for load factors greater than one by amplifying the noise levels on the acoustic hemispheres under the assumption that the loading noise is dominant and that the distribution of loading does not change significantly for small changes in thrust:

$$\Delta SPL = 20\log_{10}\frac{C_T}{C_W} \tag{4}$$

where C_W is the weight coefficient, equivalent to C_T in steady flight. For load factors less than one, no scaling of the noise levels is performed.

The ART technique does not generate noise hemispheres for hovering flight conditions, as the helicopter would not sweep a range of directivity angles without relative motion over the array. To approximate hover, a noise hemisphere is generated for zero advance ratio by averaging the sound pressure levels (on an equal energy basis) for the lowest speed flight condition measured across the fore-aft symmetry plane. Full noise spheres are then generated for each condition by reflecting the measured data on the lower half of the acoustic hemisphere to the upper half. Shepard's modified inverse distance weighting (Ref. 18) is then applied along the geodesic surface of the sphere to interpolate the SPL at five degree increments of azimuth and elevation for each condition. These data are then converted to a database file for use by the NICEOPS model.

For this paper, flight trajectories for each approach were generated from the position tracking data recorded by ANTS2, and were evaluated at 0.5 second intervals. At each point in time, the vehicle operating condition is calculated as described previously in this section. On loading the noise database, NICEOPS linearly transforms the four nondimensional parameters defining the operating condition to normalize the values in each dimension across a range from zero to one. Methods from the Computational Geometric Algorithms Library (Ref. 22) are used to construct a four dimensional Delaunay triangulation of all operating conditions in the database. The Delaunay condition of the triangulation attempts to produce triangles that are relatively uniform and not slender, making the triangulation an appropriate topology over which the conditions are interpolated.

For each point along the trajectory, the operating condition is identified and its location found inside the triangulation of conditions in the database. If the operating condition is inside the convex hull of the triangulation of conditions in the database, the four dimensional simplex containing the current operating point is identified. A barycentric interpolating weight is assigned to each of the five nodes forming the simplex. Figure 2 shows a simplified schematic of barycentric interpolation on a two-dimensional simplex. The star represents the interpolant, and points p_i the nodes of the simplex. The barycentric weights for the data located at each of the points p_i are the volume (or area in two dimensions) of the simplex formed between the interpolant and all other nodes of the simplex except for point p_i normalized by the total volume of the simplex. That is, the barycentric interpolation on a simplex with verticies $(q_1, q_2, ..., q_n)$ can be expressed as:

$$f(\vec{q}) = \sum_i w_i f(p_i) \tag{5}$$

where the weights w_i can be calculated for the n dimensional simplex as:

$$w_i = \frac{|\det(q-q_1, q_2-q_1, q_3-q_1, ..., q_n-q_1 \sim \{q_i-q_1\})|}{|\det(q_2-q_1, q_3-q_1, ..., q_n-q_1)|}, \tag{6}$$

in which q is the location of the interpolant. If the operating point lies on the face of the simplex, the dimensionality of the interpolation is reduced by one, and the interpolation is performed using only the nodes on that face. Similarly, if the operating point lies outside the convex hull of the triangulation, the nearest point on the convex hull is identified and the interpolating weights calculated from the nodes defining the face surrounding that point. The calculated barycentric weights can then be applied to all data values stored on the acoustic sphere for that condition.

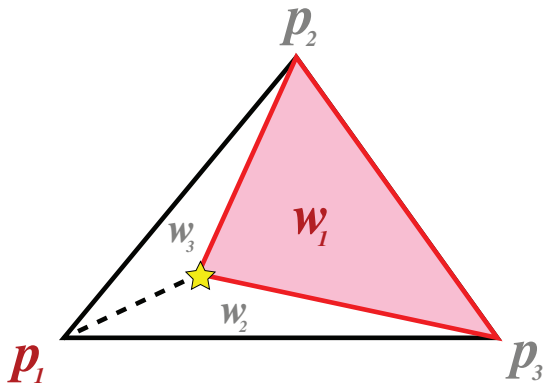

Figure 2. Barycentric interpolation on a two dimensional simplex (i.e., a triangle).

Next, for each observer point on the ground, the emission angle on the sphere is computed, and the four points on the spherical grid surrounding that point are identified. The SPL values at each of these grid points are first interpolated between operating conditions using the barycentric weights calculated from the triangulation. Next, a bilinear interpolation is performed to calculate the SPL at the desired emission angle. The noise is then propagated along a straight ray to the observer accounting for spherical spreading, atmospheric absorption, and ground effects using methods similar to those used by ART to build the original source noise hemispheres.

RESULTS

Overview of Measured Conditions

Acoustic hemispheres are formed for each steady flight condition. Figures 3 and 4 provide a summary of the acquired acoustic data for the AW139 and S-76D, respectively. At the center of each figure is an operational noise contour plot constructed using measurements from level and steady descent test points. The plot illustrates the variation of ground noise exposure level (GNEL), a metric similar to one defined by Greenwood (Ref. 3). Here, the mid-frequencies are highlighted by first band-limiting the signals from the 5th to 60th harmonic of the blade passage frequency. Note this is similar to a BVISPL metric but referred to here as mid-frequency SPL because of the unknown amount of other source mechanisms (e.g., the tail rotor) that may be present. The out-of-plane noise is then projected from the hemisphere to a ground plane at a reference height of 1,640 ft (500 m), where out-of-plane is defined here as elevation angles between -30° and -90°. Finally, a spatial average of the projection is taken and logarithmically time-duration weighted relative to a reference speed of 80 KIAS. Compensating for duration increases GNEL levels produced at conditions with lower speeds as they are typically perceived as more annoying, similar to computing sound exposure level (SEL). GNEL is computed for each measured test point denoted by the circle markers, and interpolated to produce the contour shown.

For these two aircraft, the ground noise exposure level is greatest at flight path angles in excess of -6° and biased toward lower flight speeds. If the time duration is removed, peak out-of-plane levels are found at the largest flight path angles tested for the AW139 (-10.3°). A similar result is observed for the S-76D. Being in the medium-sized vehicle class, the thrust produced by the main rotor system is large, which pushes the wake farther down and away from the rotor plane relative to lightweight helicopters (Ref. 9). As a comparison, the Robinson R-44 produces peak acoustic levels at flight path angles under -6°. In general, heavier vehicles have a higher disk loading and oftentimes lower drag-to-weight ratios, which increase the miss distance between the tip vortices and the rotor blades. It is also worth noting the density of measured test points where ground noise exposure level is greatest. If the measurement database is populated adequately around conditions near or at these noisy regions, the interpolation for the NICEOPS method will produce more accurate predictions.

While band-limiting to focus on the mid-frequency range and using the GNEL metric is instructive in terms of comparing the effective ground noise over different conditions, the simulated approaches using the NICEOPS method in the following sections will employ source hemispheres using the A-weighted sound pressure level (SPL). In an effort to provide a summary of the measurement database, several A-weighted source hemispheres are extracted from the test matrix and shown alongside the operational noise plots in Figures 3 and 4. The hemispheres across the top illustrate the measured acoustic differences in level flight at different airspeeds and demonstrate changes in noise levels by about 10-15 dB. At the highest airspeed, peak levels are associated with near in-plane emission angles. Note that while there are large differences across the level flight hemispheres, GNEL stays relatively constant. This is due to both the increase in spherical spreading on near in-plane angles (e.g., noise radiated at elevation angles of -30° are attenuated by approximately 6 dB more than -90°.) and the duration weighting (e.g., $10\log_{10}(V_{\max}/V_{\min}) \approx 5$ dB for the AW139).

Two additional sets of A-weighted hemispheres are given for each vehicle and illustrate the acoustic differences due to a change in flight path angle while maintaining approximately the same flight speed. The set of hemispheres at the low speed (about 60 KIAS) show a moderate increase in noise with flight path angle and tend to correlate with the trends found in the GNEL operational noise plots. The higher speed set (about 100 KIAS) show a similar trend, albeit with levels much greater than the low speed descents. Contrary to level flight, the descents produce peak levels at emission angles that are more out-of-plane. Even though the spheres are A-weighted, these peak directivity locations are indicative of BVI.

While a great deal of effort has gone into minimizing environmental and human effects that may introduce uncertainties in the data, there are unavoidable sources of nonideal circumstances. In an effort to provide a sense of uncertainty, a housekeeping run at the beginning and end of each day is performed. The prescribed condition is level flight at 100 KIAS and 200 ft AGL. An A-weighted source hemisphere of a single flyover is given for reference in Figure 5(a) for the S-76D. The data

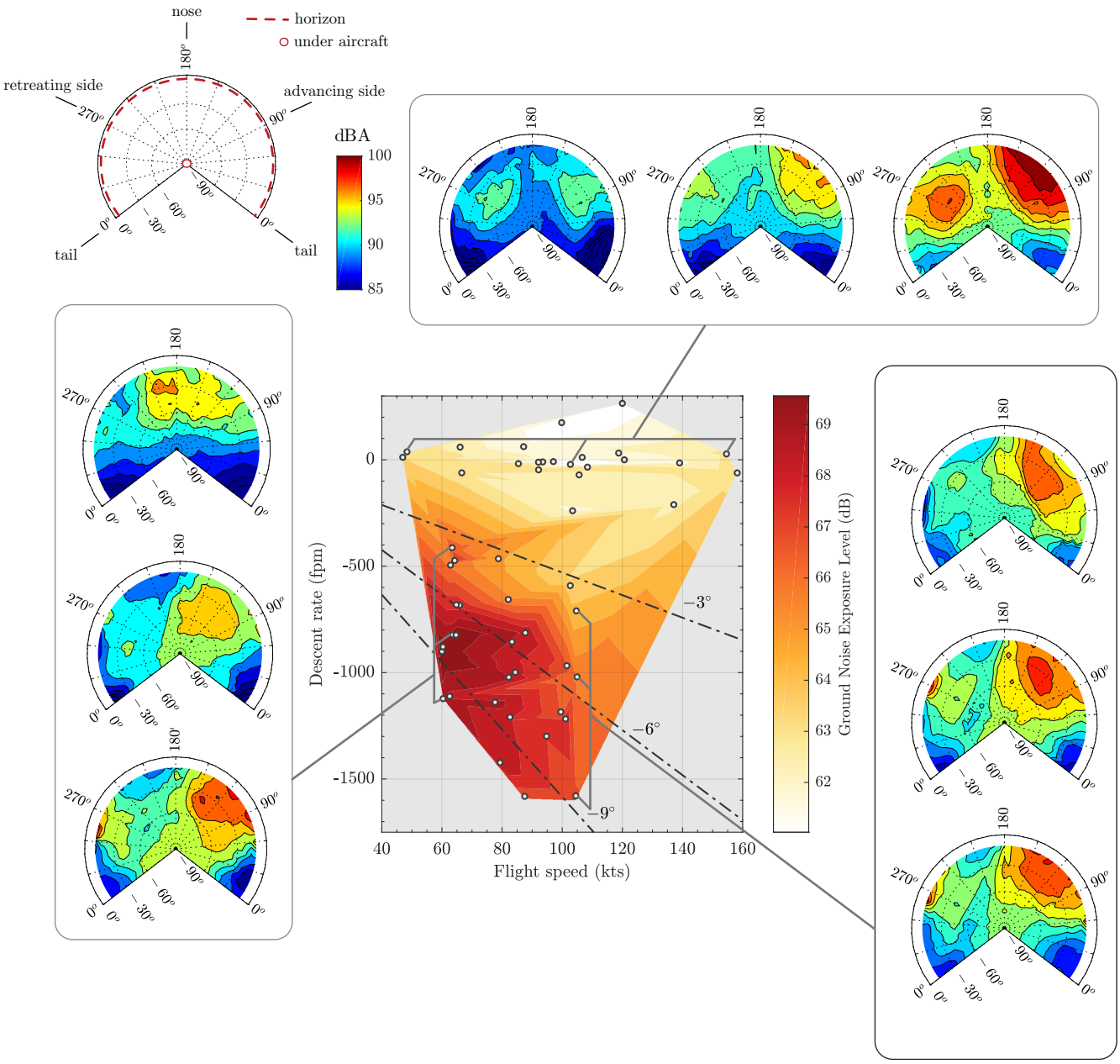

Figure 3. Operational noise plot using the ground noise exposure level acoustic metric (center) and A-weighted sound pressure level source hemispheres for the AW139.

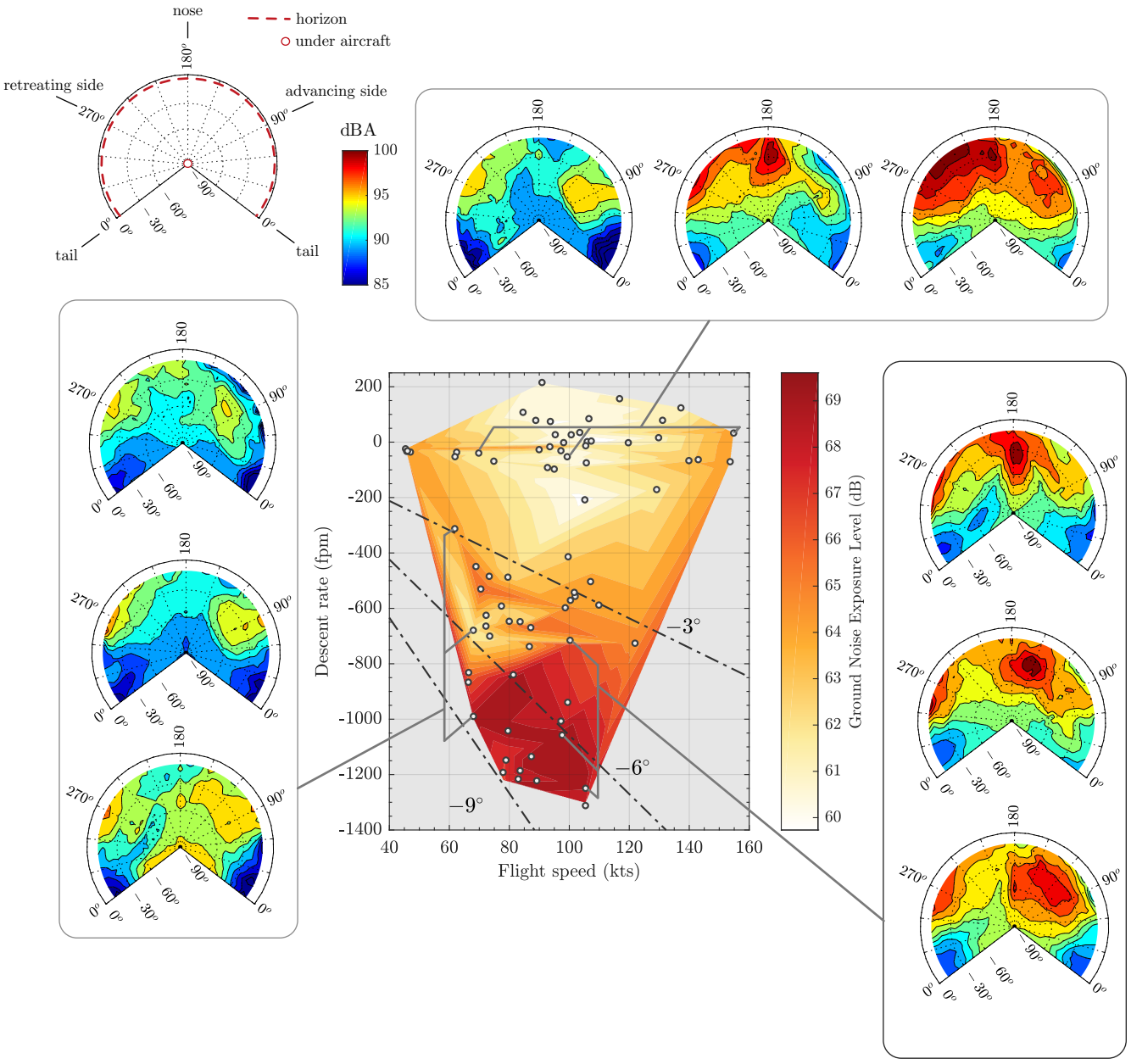

Figure 4. Operational noise plot using the ground noise exposure level acoustic metric (center) and A-weighted sound pressure level source hemispheres for the S-76D.

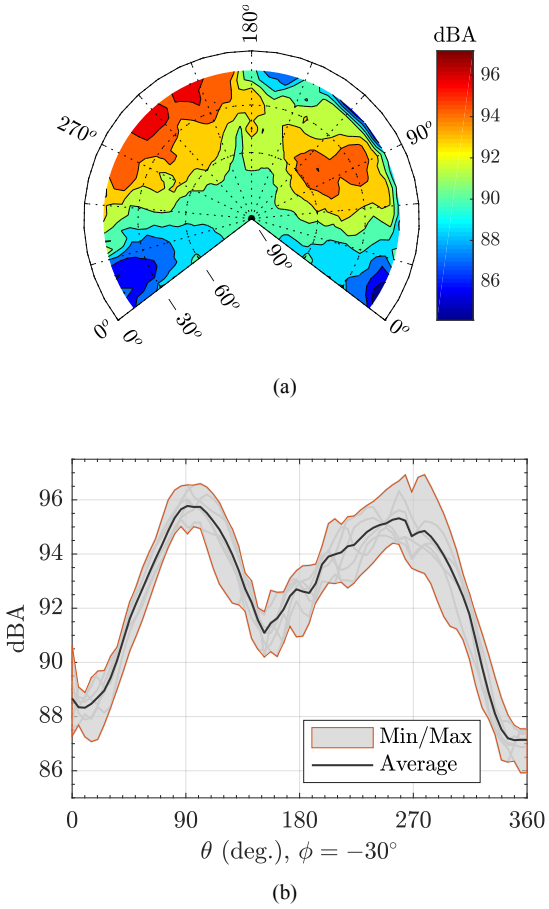

Figure 5. Example of a A-weighted hemisphere for (a) a single pass and (b) data spread at $-30°$ elevation at all azimuths for seven passes of a steady level flight at an average speed of 104 kts ($\sigma = 2.7$ kts) for the S-76D.

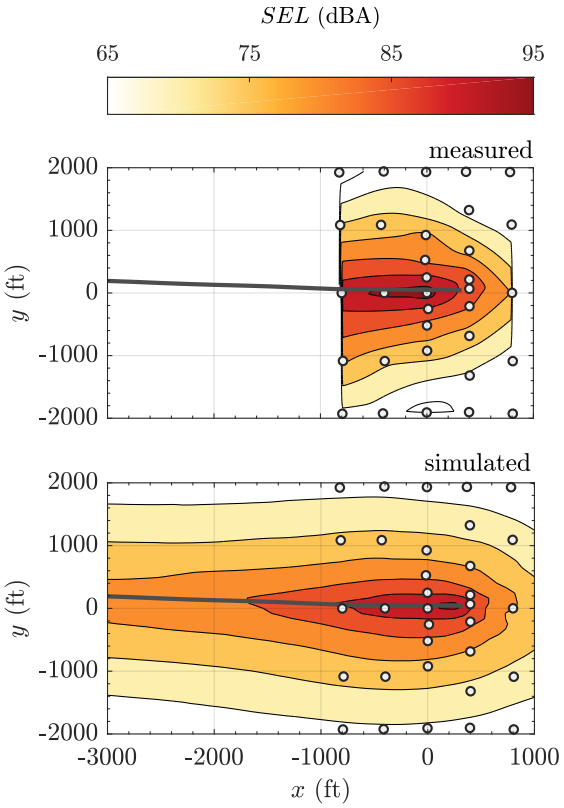

Figure 6. Comparison of measured and predicted SEL-A contours for an S-76D approach at -7.5° with initial speed of 60 KIAS.

spread is exemplified by extracting the levels over all azimuths at 30° down from the rotor plane for seven passes. The average airspeed is 104 kts with a standard deviation of 2.7 kts. Assuming the effect of differences associated with airspeed are small, the levels on any given angle deviate by approximately 1-2 dB, and up to 3 dB at a limited set of observer angles. Given these data were captured over four different test days, the associated uncertainty of the data is reasonable and very much consistent with previous tests (Refs. 9, 14).

Simulated Noise Abatement Approaches

The NICEOPS method was used to simulate extended ground noise contours for all noise abatement approaches flown for the AW139 and S-76D. In this section, selections of these simulated contours are examined with the goal of developing a better understanding of how to design effective noise abatement procedures. Figure 6 compares the extended noise contour predicted by NICEOPS to that developed by interpolating the Sound Exposure Levels (SEL) calculated directly from the measured data at each microphone for a -7.5° approach from 60 KIAS of the S-76D helicopter. The agreement between the measured and simulated noise contours is fairly good, although the measured noise contours are less regular, especially at points farther away from the flight path where uncertainty in propagation effects due to variation in atmospheric conditions, background noise, and terrain have a greater influence. Figure 7 shows the measured and simulated SEL at nine microphone stations at $x = 0$. Again, agreement is quite good—within 2 dBA SEL–for all positions except the outmost microphones and the microphone overflown by the helicopter, where small errors in the position may result in large discrepancies in SEL.

Of all simulated flight conditions for the S-76D, the one with the largest 65 dBA SEL footprint was for a run where the pilots were instructed to fly a normal approach decelerating to the intended landing point. The noise contour is plotted in Figure 8(a). Note that for this figure and the following similar figures the flight path is shown as the solid grey line. Figure 8(b) plots the nominal and effective flight path angles of the helicopter during the run. The helicopter decelerates as it travels from $x = -5000$ ft to $x = -2000$ ft, causing the effective flight path angle to be significantly steeper than the nominal flight path angle of $-6°$. Although the nominal flight path angle is above the region of greatest GNEL in the operational noise plot for the S-76D (Figure 4), the additional effect of the deceleration causes the effective flight path angle to pass through the noisy region.

The flight condition for the S-76D with the smallest 65 dBA SEL footprint was a $-5°$ approach starting from 70 KIAS. The associated noise contour is shown in Figure 9(a). Even though

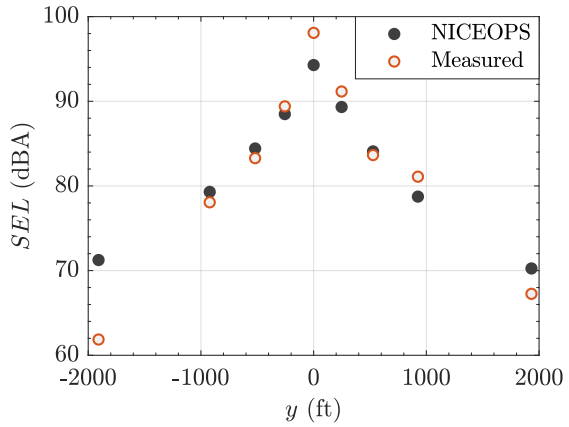

Figure 7. Comparison of measured and predicted SEL-A along $x = 0$ for an S-76D approach at -7.5° with initial speed of 60 KIAS.

the approach is slightly shallower than the normal approach shown previously, the noise contour is narrower, especially in the region farther away from the landing point. Figure 9(b) plots the variation in nominal and effective flight path angle throughout the run. During this approach procedure, the airspeed was maintained roughly constant throughout the initial portion of the approach, resulting in similar nominal and effective flight path angles through the first 4,000 ft of the approach. The deceleration was delayed until $x = -2000$ ft. At this point, the effective flight path angle passes through the noisy region of the operational noise plot, but only briefly and when at a relatively low altitude above ground.

Figure 10(a) shows the simulated noise contours for a normal approach of the AW139. As for the S-76D, this normal approach condition produced the largest 65 dBA SEL footprint of all conditions simulated. Figure 10(b) plots the nominal and effective flight path angles. A very low deceleration rate is maintained throughout the approach, which has the result of keeping the effective flight path angle of the helicopter in the noisy region of the operating envelope for the entire duration of the approach.

Figure 11(a) shows the simulated noise contours for the smallest 65 dBA SEL footprint condition for the AW139 that was flown. This condition begins from a $-7.5°$ descent at 75 KIAS. While the helicopter is initially in the noisy region of the operating envelope, a moderate deceleration quickly steepens the effective flight path angle beyond $-10°$ starting at $x = -3000$ ft. Although the operational noise plots do not contain data at these steep angles, the fact that the ground noise contour is smallest for this vehicle indicates the noisy region of Figure 3 may end close to $-10°$ at lower airspeeds found in the latter part of this approach.

CONCLUSION

Acoustic data acquired from the flight test described herein have been processed in several ways in order to provide general trends of the measurements. The operational noise plots

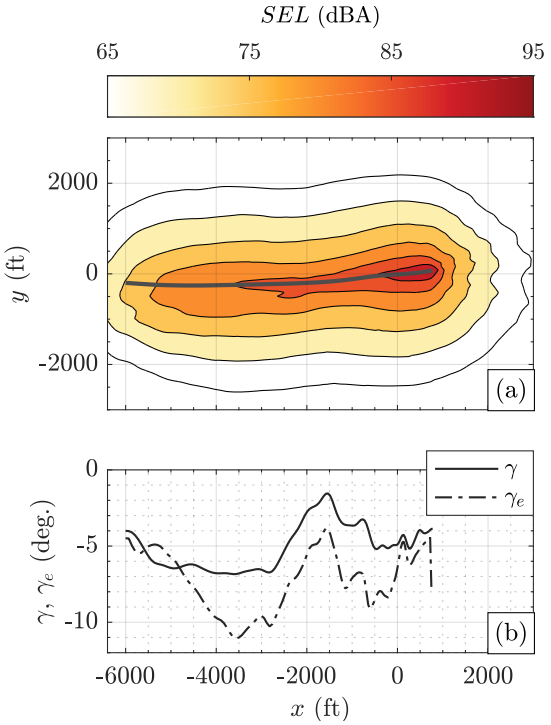

Figure 8. Predicted SEL-A contours (a) and nominal and effective flight path angle (b) for a normal approach of the S-76D.

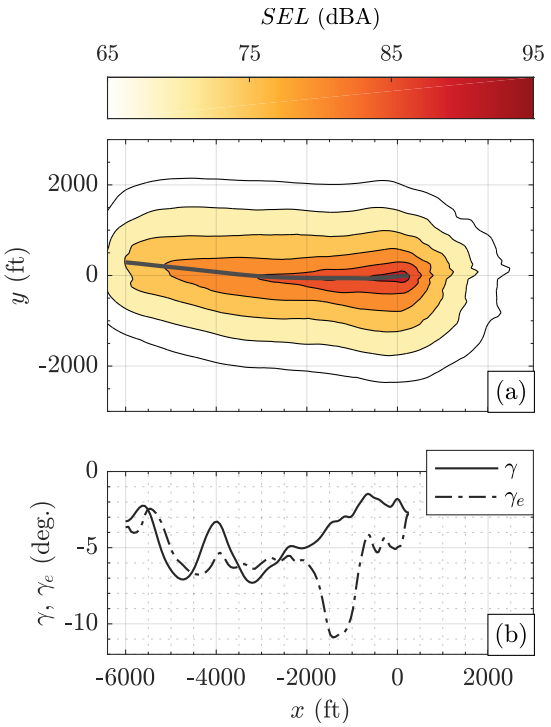

Figure 9. Predicted SEL-A contours (a) nominal and effective flight path angle (b) for a 5° approach from 70 KIAS of the S-76D.

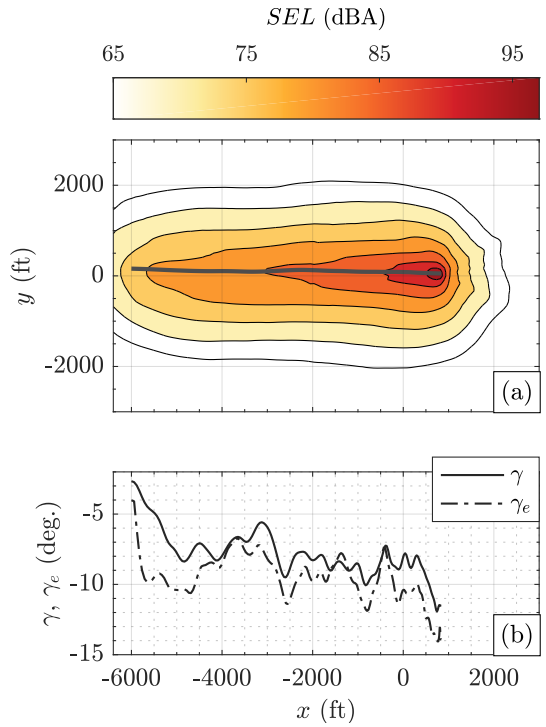

Figure 10. Predicted SEL-A contours (a) and nominal and effective flight path angle for a normal approach of the AW139.

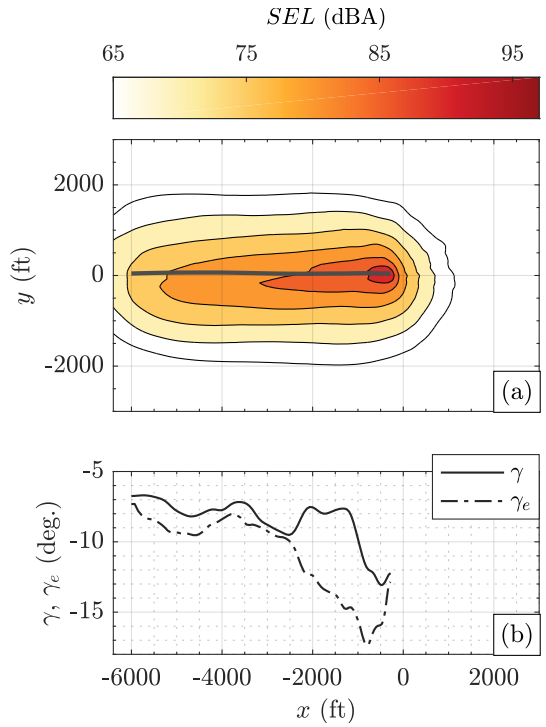

Figure 11. Predicted SEL-A contours (a) and nominal and effective flight path angle for a 7.5° approach from 75 KIAS of the AW139.

contain useful information about how the noise generation of the helicopter varies as the flight condition of the vehicle changes, independent of the geometry of the approach trajectory. Individual source hemispheres demonstrate the differences in both levels and directivity under constant flight conditions. For both the AW139 and S-76D, in-plane noise increases with airspeed in level flight. Out-of-plane noise is shown to increase with descent angle and peak near or at the steepest angles tested, particularly at high flight speeds.

The influence of longitudinal acceleration is found to have a powerful effect on the aerodynamic, and therefore acoustic, state of the helicopter. Operators must be aware of these effects in order to plan effective low noise flight trajectories using these data. The effective flight path angle exceeded the range of nominal flight path angles measured for nearly every noise abatement approach condition tested. Because of the relatively high disk loading and low drag-to-weight ratios of the medium-sized helicopters tested and discussed herein, the wake convects relatively far beneath the rotor in level flight, and the high BVI noise region often occurs during the steepest angles achievable during steady descending flight. However, even a modest deceleration can result in the helicopter rotor operating at steeper angles of attack. In order to best provide tools and information to help operators "fly neighborly," new flight procedures or modeling methods should be developed to characterize the noise radiation during these routinely encountered flight conditions.

ACKNOWLEDGMENTS

The authors would like to thank the team for their outstanding dedication and hard work that made this test possible. NASA Langley: Susan Gorton and C. Benny Lunsford. Analytical Mechanics Associates: H. Keith Scudder, Jeff Davis. FAA Office of Energy and the Environment: Rick Riley. Volpe: Juliet Page, Amanda Rapoza, Robert Downs. FAA Technical Center: Charles Johnson. U.S. Army: Oliver Wong. NJ Forest Fire Service: John Wimberg, Rob Gill, Sal Cicco.

REFERENCES

1. Lin II, R.-G., "L.A. County backs federal restriction of low-flying helicopters," *LA Times*, November 2011.

2. Vail, E., "Adopt Local Law- Amending Chapter 75 (Airport) of the Town Code Regulating Nighttime Operation of Aircraft at East Hampton Airport," East Hampton Town Board Resolution 2015-411, 2015.

3. Greenwood, E., "Helicopter Flight Procedures for Community Noise Reduction," American Helicopter Society 73rd Annual Forum, May 2017.

4. Jacobs, E., O'Connell, J., Conner, D., Rutledge, D., Willson, M., Shigemoto, F., Chen, R., and Fleming, G., "Acoustic Flight Testing of a Boeing MD Explorer and a Sikorsky S-76B Using a Large Area Microphone Array," American Helicopter Society Technical Specialists Meeting for Rotorcraft Acoustics and Aerodynamics, 1997.

5. Visser, H., Pavel, M., and Tang, S., "Optimization of Rotorcraft Simultaneous Noninterfering Noise Abatement Approach Procedures," *Journal of Aircraft*, Vol. 46, (6), 2009, pp. 2156–2161.

6. Speigel, P., Buchholz, H., and Pott-Pollenske, M., "Highly Instrumented BO105 and EC135-FHS Aeroacoustic Flight Tests including Maneuver Flights," American Helicopter Society 61st Annual Forum, August 2005.

7. Ishi, H., Gomi, H., and Okuno, Y., "Helicopter Flight Tests for BVI Noise Measured Using an Onboard External Microphone," AIAA Flight Mechanics Conference and Exhibit, August 2005.

8. Greenwood, E., Schmitz, F., Gopalan, G., and Sim, B., "Helicopter External Noise Radiation in Turning Flight: Theory and Experiment," American Helicopter Society 63rd Annual Forum, May 2007.

9. Watts, M., Greenwood, E., Smith, C., and Stephenson, J., "Noise Abatement Flight Test Data Report," NASA TM 2019-220264, 2019.

10. Pascioni, K., Greenwood, E., Watts, M., Smith, C., and Stephenson, J., "Medium-Sized Helicopter Noise Abatement Flight Test Data Report," *in progress*, NASA TM 2020, 2020.

11. Stephenson, J., Watts, M., Greenwood, E., and Pascioni, K., "Development and Validation of Generic Maneuvering Flight Noise Abatement Guidance for Helicopters," American Helicopter Society 76th Annual Forum, October 2020.

12. Page, J. A., Wilmer, C., Schultz, T., Plotkin, K. J., and Czech, J., "Advanced Acoustic Model Technical Reference and User Manual," Wp-1304, serdp, 2009.

13. Conner, D., Burley, C., and Smith, C., "Flight Acoustic Testing and Data Acquisition for the Rotorcraft Noise Model (RNM)," American Helicopter Society 62nd Annual Forum, May 2006.

14. Watts, M., Greenwood, E., Smith, C., Snider, R., and Conner, D., "Maneuver Acoustic Flight Test of the Bell 430 Helicopter Data Report," NASA TM 2014-218266, 2014.

15. "Method for the Calculation of the Absorption of Sound by the Atmosphere," Standard ANSI S1.26-1995, American National Standards Institute, Inc., New York, New York, 2004.

16. Delany, M., and Bazley, E., "Acoustical properties of fibrous absorbent materials," *Applied acoustics*, Vol. 3, (2), 1970, pp. 105–116.

17. Chien, C., and Soroka, W., "Sound propagation along an impedance plane," *Journal of Sound and Vibration*, Vol. 43, (1), 1975, pp. 9–20.

18. Shepard, D., "A Two-Dimensional Interpolation Function for Irregularly-Spaced Data," ACM '68, Proceedings of the 1968 23rd ACM National Conference, 1968. DOI: 10.1145/800186.810616

19. Greenwood, E., and Rau, R., "A Maneuvering Flight Noise Model for Helicopter Mission Planning," *Journal of the American Helicopter Society*, Vol. 65, (2), 2020, pp. 1–10.

20. Schmitz, F. H., Gopalan, G., and Sim, B. W.-C., "Flight-Path Management/Control Methodology to Reduce Helicopter Blade-Vortex Interaction Noise," *Journal of Aircraft*, Vol. 39, (2), 2002, pp. 193–205.

21. Greenwood, E., "Estimating Helicopter Noise Abatement Information with Machine Learning," American Helicopter Society 74th Annual Forum, May 2018.

22. Hert, S., and Seel, M., "dD Convex Hulls and Delaunay Triangulations," *CGAL User and Reference Manual*, CGAL Editorial Board, 5.0.2 edition, 2020.